University of New Hampshire
University of New Hampshire Scholars' Repository

Center for Coastal and Ocean Mapping | Center for Coastal and Ocean Mapping

5-2002

Geometric and Radiometric Correction of Multibeam Backscatter Derived from Reson 8101 Systems

Jonathan Beaudoin
University of New Hampshire, Durham

J.E. Hughes Clarke
University of New Brunswick

Edward J. Van den Ameele
USGS

James V. Gardner
University of New Hampshire, Durham, jim.gardner@unh.edu

Follow this and additional works at: https://scholars.unh.edu/ccom

 Part of the Oceanography and Atmospheric Sciences and Meteorology Commons

Recommended Citation

Beaudoin, Jonathan; Clarke, J.E. Hughes; Van den Ameele, Edward J.; and Gardner, James V., "Geometric and Radiometric Correction of Multibeam Backscatter Derived from Reson 8101 Systems" (2002). *Canadian Hydrographic Conference*. 242.
https://scholars.unh.edu/ccom/242

This Conference Proceeding is brought to you for free and open access by the Center for Coastal and Ocean Mapping at University of New Hampshire Scholars' Repository. It has been accepted for inclusion in Center for Coastal and Ocean Mapping by an authorized administrator of University of New Hampshire Scholars' Repository. For more information, please contact Scholarly.Communication@unh.edu.

GEOMETRIC AND RADIOMETRIC CORRECTION OF MULTIBEAM BACKSCATTER DERIVED FROM RESON 8101 SYSTEMS

Beaudoin, J.D.[1], Hughes Clarke, J.E. [1], Van Den Ameele, E.J.[2] and Gardner, J.V. [3]

1: Ocean Mapping Group (OMG), Department of Geodesy and Geomatics Engineering, University of New Brunswick
2: National Ocean Service, National Oceanic and Atmospheric Administration (NOAA)
3: United States Geological Survey (USGS), Menlo Park, CA

ABSTRACT

A common by-product of multibeam surveys is a measure of the backscattered acoustic intensity from the seafloor. These data are of immense interest to geologists and geoscientists since maps of the acoustic backscatter strength can be used to infer physical properties of the sea bottom, such as impedance, roughness and volume inhomogeneity. Before such maps can be created from multibeam acoustic backscatter data, however, two tasks must be performed:

1. The data must be geographically registered using the bathymetric profile collected by the multibeam (which accounts for full orientation and refraction), as opposed to using the traditional flat-seafloor assumption. This allows us to additionally calculate the true grazing angle.
2. The signal intensities must be reduced to as close a measure of the backscatter strength of the seafloor as possible by radiometrically correcting the data on a ping-by-ping basis for variables such as transmission power, beam pattern, receiver gain, and pulse length.

The purpose of this research project is to develop software tools to perform the above corrections for a massive backlog of RESON SeaBat 8101 multibeam data, as collected by the NOAA ship Rainier. While the backscatter logged by the multibeam systems is not of prime importance to NOAA's hydrographic charting mandate, they recognize the potential value of this data to the work of other sister agencies such as the U.S. Geological Survey (who is funding this project). The particular problems encountered with these data are that:

- Up to the end of 2001 field season, the backscatter data acquired by this system were collected from dedicated receiver beams, separate from those used for bathymetry. This receive beam is broad in the elevation plane (similar to a sidescan sonar) so that the variation in elevation angle

with time must be indirectly inferred from the corresponding bathymetric profile.
- As some backscatter data are collected from slant-ranges beyond which bathymetric data are acquired, for that case the imaging geometry must be either inferred using a simple slope model, or derived from neighbouring swaths.

Results of the application of full geometric and radiometric corrections will be presented.

INTRODUCTION

While designed primarily for bathymetric profiling, multibeam sonars have the potential to produce backscatter imagery of acceptable quality for seabed interpretation. Currently, there are three approaches to logging acoustic backscatter with a multibeam system [Hughes Clarke, 1998]:

1. Form two additional wide angle receive beams to port and starboard that log a sidescan-like time series of intensities.
2. Log a single backscatter value with each beam, either taken as the maximum intensity at bottom detect, or an average intensity centered on the bottom detect in the time series.
3. Log a series of intensities with each beam, again, centered on the bottom detect.

The first approach is limited since the backscatter information is divorced completely from the bathymetric profile provided by the beam solutions. A flat seafloor assumption could be used to slant-range correct the data, however, it is preferable to use the simultaneously collected bathymetric profile. One possible method of performing the slant-range correction is to map portions of the time-series between beam solutions on the seafloor. This is a fairly robust method, yet it requires additional post-processing; further to this, the wide-angle receive beam cannot discriminate between two echoes arriving from different directions at the same time.

The second method improves upon the first since the intensity is logged for each beam and can be directly geo-referenced using the positioned beam footprint (azimuth and depression angle of the beam, along with two-way travel time (TWTT)). The drawback of this approach is that potentially useful spatial information is discarded in the process of reducing the backscatter time-series surrounding the bottom detect of each beam to a single value.

The third technique overcomes the weaknesses of the first two methods in that: (1) the individual time series are directly associated with a portion of the bathymetric profile and are therefore much easier to correct for slant-range, (2) it allows for across-track resolution of seafloor features with spatial frequencies higher than the beam spacing since a portion of the time series is preserved for

each beam, and (3) common slant-range (layover) is restricted to the dimension of a single beam.

Since multibeam sonars are designed primarily for bathymetry, the proper reduction of the output backscatter data is of secondary importance and is often neglected by system designers. Users of multibeam backscatter are thus faced with a myriad of possible corrections. The radiometric corrections involved in this project are standard corrections that must be performed, to some extent or another, on backscatter data from most multibeam systems. As an example, the following corrections were identified for reduction of backscatter data from Simrad EM1000 systems (after Hughes Clarke et al. [1996, p. 619]):

1. Measurement of true seafloor slope.
2. Variations between the predicted and actual transmit beam patterns.
3. Variations between the apparent and true grazing angle due to refraction.
4. Aspherical focusing.
5. Irregular attenuation of the signal due to variations in local water mass properties.
6. Removal of angle-varying correction based on Lambertian model.

Since multibeam systems vary widely in the types of reductions applied to the backscatter data at collection time, not all of the corrections listed above will necessarily apply to the reduction of data in this paper.

The purpose of this research project is to develop software tools to perform a geometric and radiometric correction of acoustic backscatter from RESON SeaBat 8101 multibeam data, as collected by the NOAA Ship Rainier, a hydrographic vessel owned and operated by NOAA. The systems, as installed on two of the Rainier's six survey launches, are outfitted with a sidescan option, allowing for the logging of acoustic backscatter data from dedicated port and starboard receive beams, separate from the bathymetric beams (first method as described earlier). In addition to the trace data provided by the sidescan option, a single, beam-averaged intensity value is logged with each beam in the bathymetry packet (second method). This paper will show the results of the full geometric and partial radiometric correction of both the trace and beam-averaged intensities and the production of acoustic backscatter maps from both of these data.

METHODOLOGY

The SeaBat 8101 is a 101 beam, 240 kHz shallow water multibeam system and is typically deployed on a 10-metre survey launch. While the transmit transducer is a linear array, the receive transducer is an arcuate array with receive beams spaced in an equi-angular manner. Each beam has a beamwidth of 1.5 degrees (along and across-track), giving a maximum swath width of 7.4 x water depth in ideal conditions [RESON, 2000]. Several upgrade options are available with the basic system, one being the sidescan option. With

this option, separate port and starboard receive beams are formed and generate a sidescan like time series of intensities (refer to Figure 1). While the SeaBat 8101 is not roll-stabilized, it is capable of pitch stabilization, however this option has not been installed on the Rainier multibeam systems. Recent firmware upgrades from RESON have implemented the third method of logging backscatter, allowing for the logging of 'snippets' of acoustic backscatter for each beam [Lockhart *et al*., 2001]. This logging format is not treated in this paper as it is not yet installed on NOAA launches; it is, however, the focus of current research in the OMG.

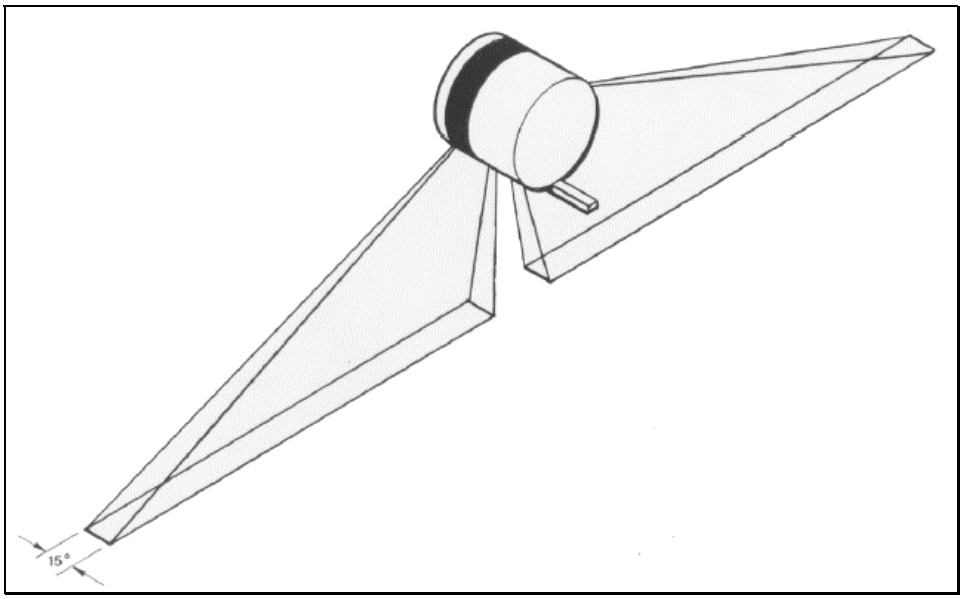

Figure 1. Sidescan beam geometry (from RESON [2000, p. 4-3]). Boresite of both beams is 43.5° off nadir. Beamwidth in the elevation plane is 67.2° (implying a 19.2° null at nadir). Note that while the along-track receive beamwidth is 15°, the transmit beamwidth is 1.5° [RESON, 2000].

Compared to other sonars, the acoustic backscatter logged by the SeaBat 8101 is in a relatively uncorrected state. If backscatter imagery were to be produced using the data, the imagery would suffer from visual artifacts, all due to changes in power level, gain and pulse length. These artifacts often appear as across-track banding, as seen in Figure 2, where slant-range intensities are stacked to create a port and starboard looking sidescan image. Being artifacts of dynamic signal parameters, these bands are not reflective of changes in bottom type and hinder analysis, geological or otherwise.

A radiometric correction must be performed even in the event that a line of data is collected with invariant power and gain settings. Although imagery from such a line would appear to be satisfactory when viewed in isolation, the effect of differing signal parameters between adjacent lines of data becomes apparent when one mosaics the backscatter from several lines of data together. Such a mosaic is presented in Figure 3, which shows a 5400 metre by 3300 metre

region on the western shore of Alaska's Resurrection Bay (these data being the test set used throughout this paper). The image was created in three steps: (1) a slant-range correction was performed using the nadir depth and a flat seafloor assumption, (2) backscatter values were approximately geo-referenced using the time-tagged position of the ping and the vessel's course made good (CMG), and (3) pixels in the output image were assigned a value based on their proximity to a line of data. Figure 4 displays a larger scale subset of the same area; although geological features are discernible throughout the image, there is clearly room for improvement. In addition to across-track banding in individual survey lines, note the inconsistent intensities between adjacent lines.

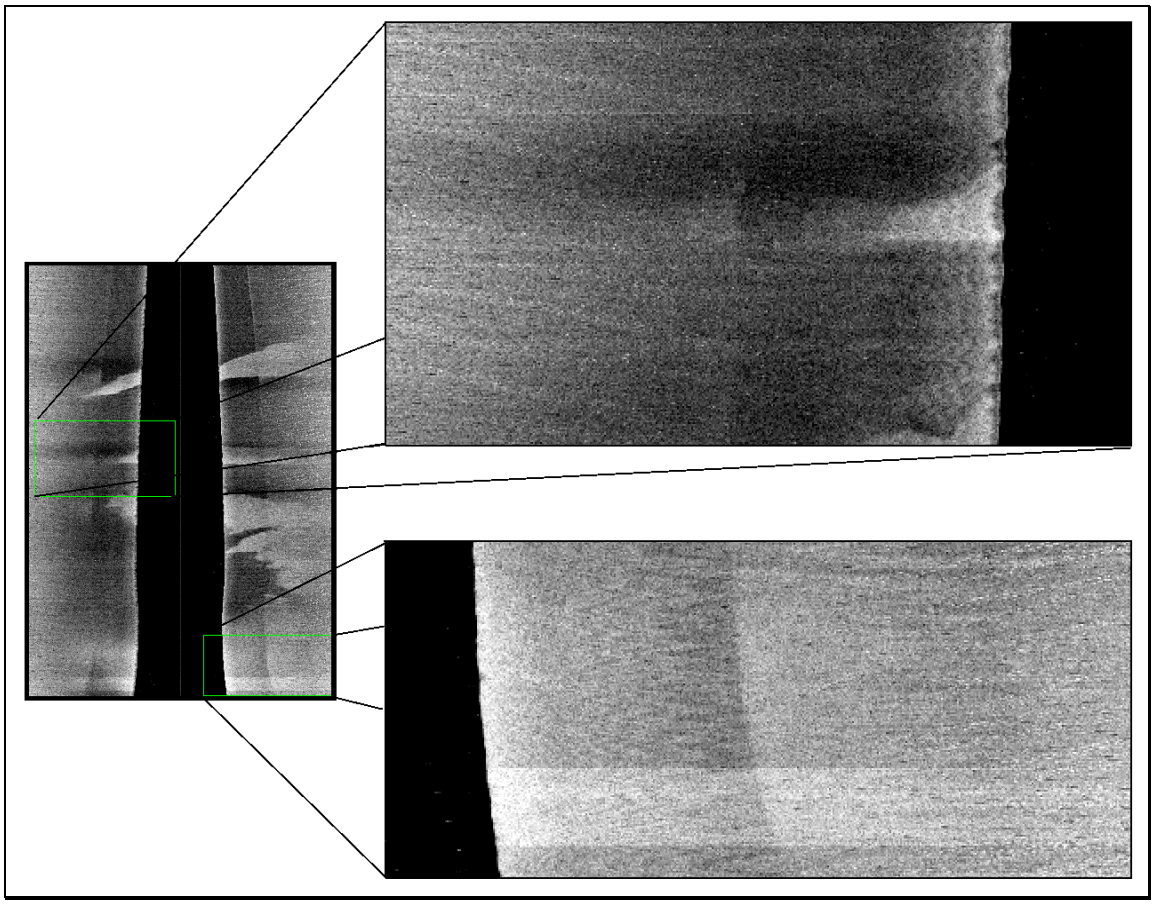

Figure 2. Banding artifacts in slant-range imagery from a RESON 8101 multibeam. The upper right image demonstrates Automatic Gain Control (AGC) being applied as sonar passes over high-backscatter targets at nadir. Gain is ramped down in this case and off-nadir targets appear darker in the image. The lower right image shows the effect of an increase in power. In typical survey operations onboard the Rainier launches, the operators control the power manually while the sonar performs AGC.

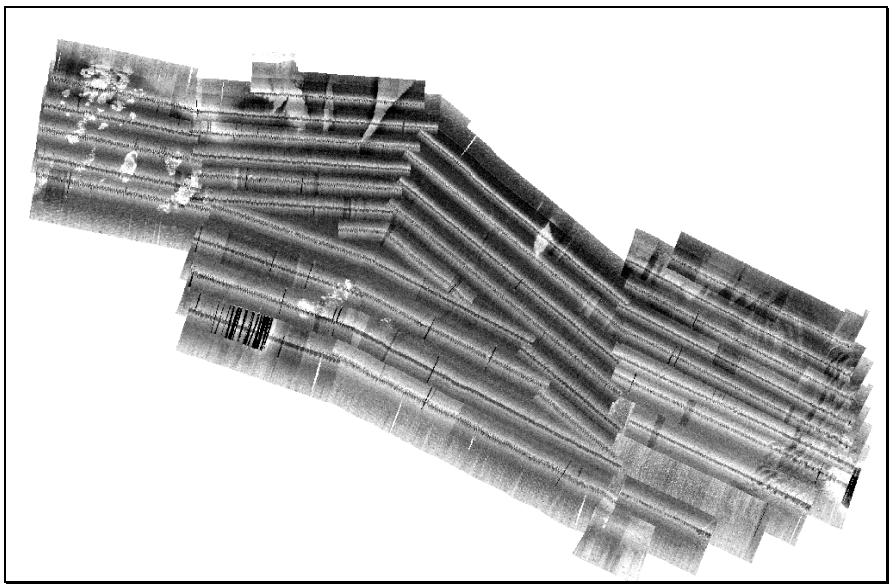

Figure 3. Mosaic of slant-range corrected SeaBat 8101 data, collected in August 2001 in Resurrection Bay (Alaska, U.S.A). Area is 5400 m x 3300 m with North oriented to the right. The shallowest waters in this area are found in the north-east (right), as evidenced by the decreased line-spacing.

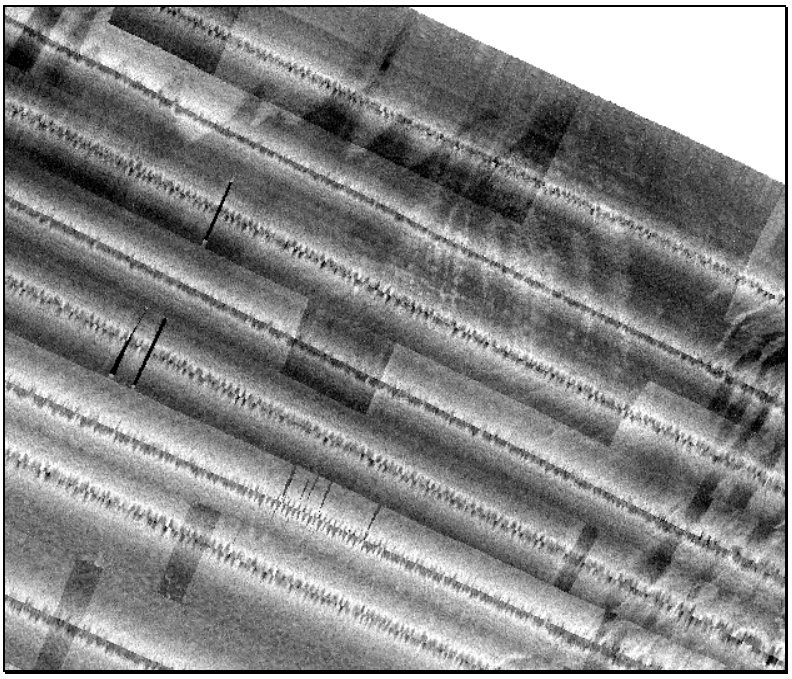

Figure 4. Large Scale Mosaic of SeaBat 8101 data. Note inconsistent intensities between survey lines, corresponding to use of different power levels from one line to the next (power levels set manually by operator). In this case, a lower power setting is used in the shallower areas (upper section of the image).

Overall Procedure

The ultimate goal of this research project is to produce software that allows for the creation of radiometrically and geometrically correct acoustic backscatter data as logged by the RESON 8101 systems as installed on the NOAA ship Rainier. There are two major tasks associated with this goal: (1) convert the raw XTF (eXtended Triton Format) data into OMG format, and (2) modify existing OMG software to perform the geometric correction of the data. Due to the fact that the raw acoustic backscatter data were uncorrected for power and gain settings, it was essential at the early stages of the project to determine whether it was possible to use the logged power and gain settings in the RESON bathymetry packets to correct the trace data (since the two are stored in different XTF packets). Thus, the following overall research methodology was developed:

1. Feasibility analysis: Can the power and gain effects be removed using the settings as logged in the bathymetry packets?
2. Data conversion: Read raw XTF data; convert it into OMG data structures.
3. Geometric correction of trace data: Modify existing OMG software to accommodate SeaBat 8101 data. Apply findings of Step 1 and radiometrically reduce the data during the slant-range correction process.

Each of these steps is discussed in more detail below, followed by an examination of the results of the overall process.

Feasibility Analysis of Radiometric Correction

It is prudent to confirm the assumption that the banding artifacts seen in Figures 3 and 4 are indeed caused by changes in power and gain settings on the sonar; this is done by examining the typical backscatter, power and gain values from one of the data files, as shown in Figures 5 and 6. By examining areas in the graphs of Figures 5 and 6 closely, one can visually correlate the changes in

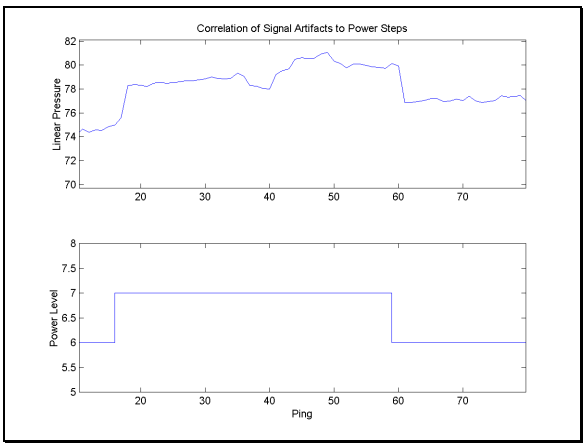

Figure 5. Visual qualitative correlation of backscatter steps to changes in transmit power.

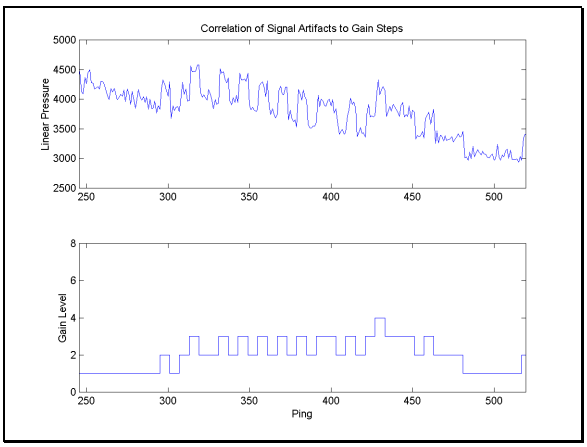

Figure 6. Visual qualitative correlation of backscatter steps to changes in receiver gain.

power and gain to steps in the average signal backscatter. The same parameters for the entire file are shown in Figure 7.

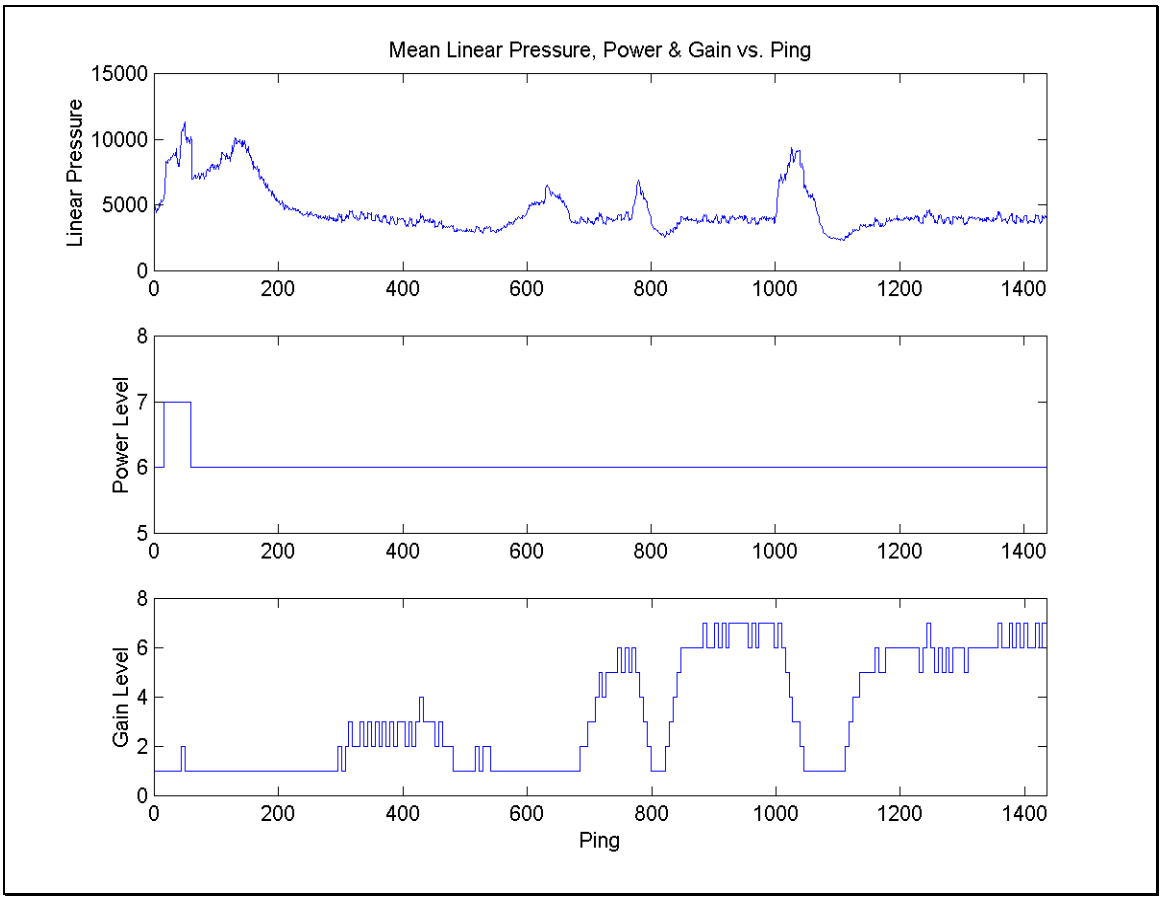

Figure 7. Typical backscatter, power and gain values in an XTF file.

It is clear from Figures 5, 6 and 7 that the artifacts and signal parameters are indeed correlated, thus the actual reduction of the signal can be attempted using the power and gain settings. Under the assumption that the sonar records the backscatter in units of linear pressure, the data must first be converted to linear intensity; this accomplished, one then computes the logarithmic intensity of the signal. Note that the logarithmic value is referenced to an unknown source level, assumed at this point to be unity (although this must be accounted for eventually, cf. section on Further Research). The recorded power levels are in steps of 3 dB, whereas the gain levels are in steps of 1 dB [RESON, 2000]. Each ping can be reduced to a common power and gain level by simply subtracting these values from the entire signal as in (Eq. 1):

$$S_{reduced} = 10 \cdot \log(S_{raw}^2) - 3 \cdot power - gain, \qquad \text{(Eq. 1)}$$

where S denotes a single sample of the return signal.

A slant-range image of a single data file is shown in its raw and corrected states in Figures 8 and 9, respectively. To aid in the visual correlation of artifacts to sonar settings, the power, gain and pulse length settings have been plotted in the upper section of the images. Note that banding artifacts are introduced into the water column portion of the signal after the reduction. It is correct to remove the power settings only for reverberation or targets within the water column. In the case of gain, any return that correlates with the gain adjustment (and not power) would indicate environmental or electronic noise. In any case, the introduction of artifacts into the water column is of little concern since this portion of the signal is discarded during slant-range correction.

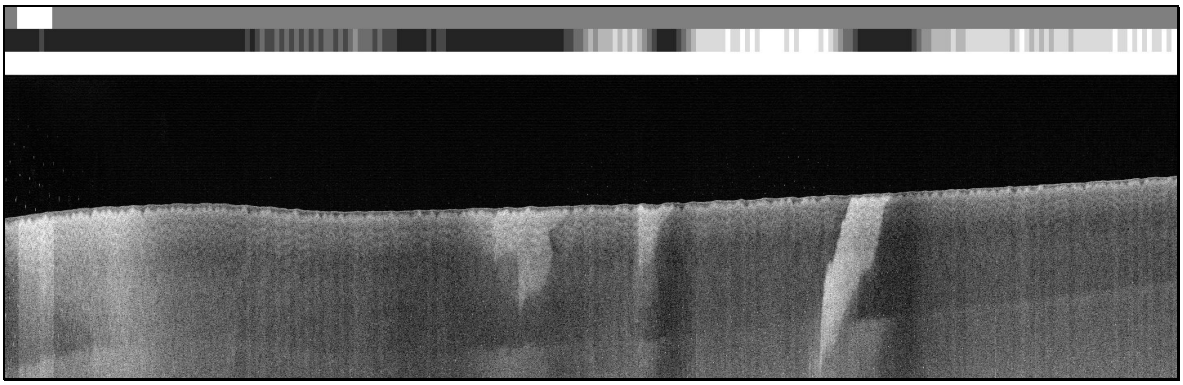

Figure 8. Starboard backscatter, uncorrected. In addition to the artifacts mentioned in Figure 2 (same image), note the high frequency banding artifacts due to rapid variation of receiver gain (AGC). The three rows stretched across the upper section of the image represent the power, gain and pulse width settings as recorded by the sonar.

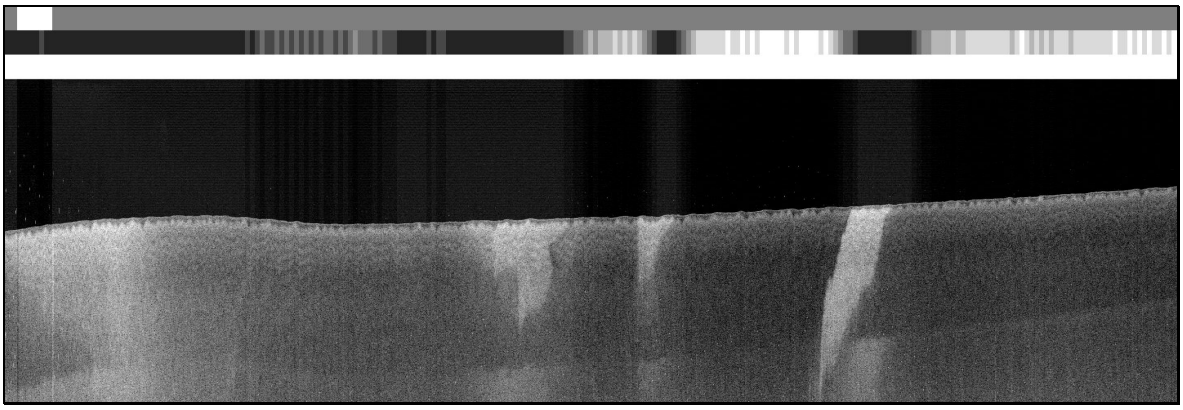

Figure 9. Starboard backscatter, corrected for power and gain settings. The AGC driven high-frequency banding artifacts have been removed in addition to the bright band in the left hand side of the image (due to a power increase). Of interest in this image are the banding artifacts that are introduced into the water column after the correction and also the strong presence of a multiple reflection.

While most of the banding artifacts were removed from the slant-range imagery, portions of the original artifact persisted with the remaining bands occurring immediately following power and gain setting changes. This is evident in the far left of Figures 8 and 9. The bright band in the far left of Figure 8 has

been removed in Figure 9, yet there remains a slight residual artifact measuring only a few pixels wide. Figures 10 and 11 portray the residual bands graphically by plotting the average backscatter per ping, before and after the removal of the power and gain levels from the signal. Note that after an increase in the power or gain level, the residual bands immediately following are too 'dark' compared to their neighbours. The converse is also true: residual bands immediately following a drop in power or gain are too 'bright' as compared to their neighbours before and after the level change. This suggests that new power and gain settings are logged immediately but are applied slightly later in time. A thorough investigation of the dataset yielded a constant power lag of two pings and a gain lag of one ping, i.e. a new power setting is logged immediately, but is applied two pings later in time. Algorithms developed up to this point were modified to account for the observed lag values. For the time being, it is assumed that the lag values are constant, i.e. do not change with ping rate; potential problems may arise if the lag is a function of ping-rate. The cause of the lag is unknown at the time of this writing but is under investigation. Similar problems have been seen with RESON 9001 systems and were due to the time required to charge capacitors while increasing power [Hughes Clarke, 1997].

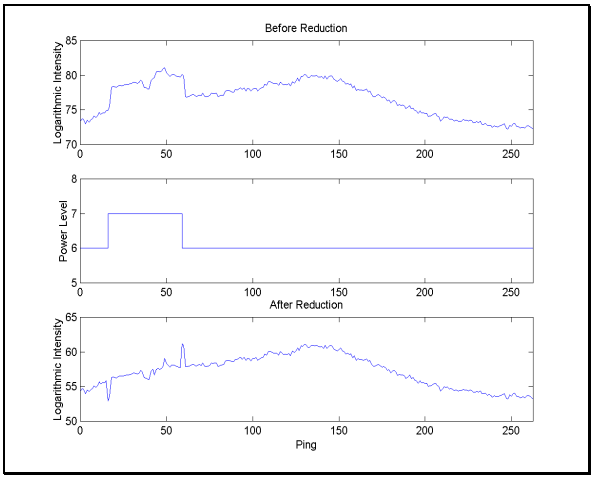

Figure 10. Residual power artifacts. The downward spike prior to power step implies that power level is being corrected for too early. This is confirmed with the upward spike after the power drop.

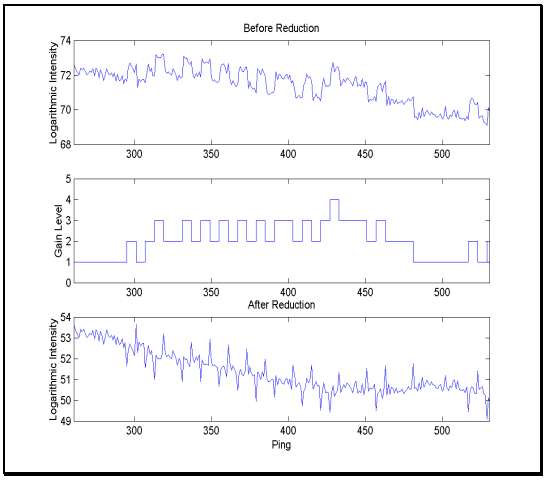

Figure 11. Residual gain artifacts. Again, direction of the spikes signal that the new gain values are applied too early in time.

Data Conversion

This second stage of the process involved writing binary file converters that read raw XTF data and converted it into the OMG format. The major difference between XTF and OMG formats is that XTF stores all data in one binary file, whereas the OMG format has several files (bathymetry, backscatter, and vessel orientation). Preliminary software involved the creation of algorithms to provide pseudo-random access to the XTF packets via a file index. This significantly reduced the complexity of the conversion algorithms since packet

types could be dealt with one at a time. The following list summarizes the major steps in the conversion algorithm:

1. Determine reference time (milliseconds since 1970).
2. Retrieve power and gain settings for all pings, shift by observed lag.
3. Match backscatter packets to bathymetry packets.
4. Write out all bathymetry and backscatter data to file.
5. Write out attitude data to file.

Once converted, it was necessary to compute the final position of each beam's footprint on the seafloor since the SeaBat only stores the raw TWTT and angle and does not perform a full geometric positioning solution for each beam. This second process is separate from the aforementioned conversion process and serves to update the OMG beam structures within the bathymetry file to arrive at a final computed position of the center of the beam footprint on the seafloor. This is computed using a plane-plane intersection (since the system is neither pitch nor roll stabilized) and involves merging the attitude data at time of transmit and receive for each beam as well as the sound velocity profile to arrive at a 3-D position vector for each beam in the locally level coordinate system. Existing OMG software was modified to accommodate the converted SeaBat 8101 data.

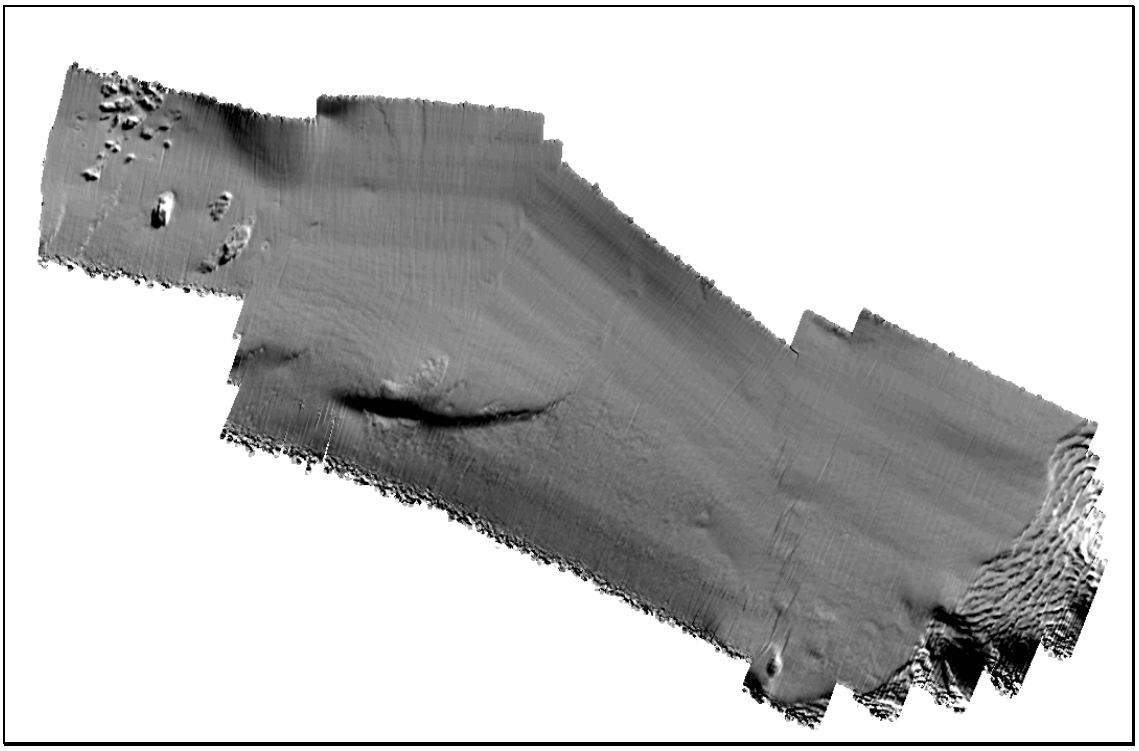

Figure 12. Sun-illuminated topography of study area (5-metre pixel size). Soundings were reduced using observed tides from Agnes Cove, a short distance to the south.

Once converted, it is then possible to use standard OMG software to clean the bathymetry and create a weighted-mean DTM from the soundings as shown in Figure 12. While the dataset must be further geometrically corrected for vessel offsets and misalignments, these were considered negligible for the production of preliminary maps of acoustic backscatter and were not applied (refer to Table 1).

Table 1. Vessel configuration parameters (offsets and misalignments are between the trandsucer and MRU).

X offset	0.00 m
Y offset	0.79 m
Z offset	0.52 m
Roll	0.10 degrees
Pitch	-1.00 degrees
Heading	1.00 degrees
Navigation latency	0.30 seconds

Geometric correction

The geometric correction consists of converting a slant-range strip of backscatter imagery to its corresponding ground range. The methodology employed is based on the fact that one can ascertain the time of ensonification of any position along the profile in the locally level coordinate system from the TWTTs and the across-track offsets of adjacent beams (refer to Figure 13). The procedure is as follows:

1. Construct an across-track array of the same resolution as the desired horizontal-range strip. For each beam, populate its appropriate cell in the strip with its TWTT (indexed by the beam's across-track offset).
2. Interpolate between the TWTTs of each beam where necessary.
3. Use the times as an index into the backscatter time series in order to populate a horizontal-range cell with the correct slant-range intensity.

Note that port and starboard trace data are handled separately in that port beams index into the port trace and vice versa. This method was originally incorporated into the OMG software library to process data from Atlas systems (which also log a time-series of intensities) and required only slight modification in order to process the SeaBat data. This method will compress and stretch the slant-range data correctly except in overlay conditions [Hughes Clarke, 1998].

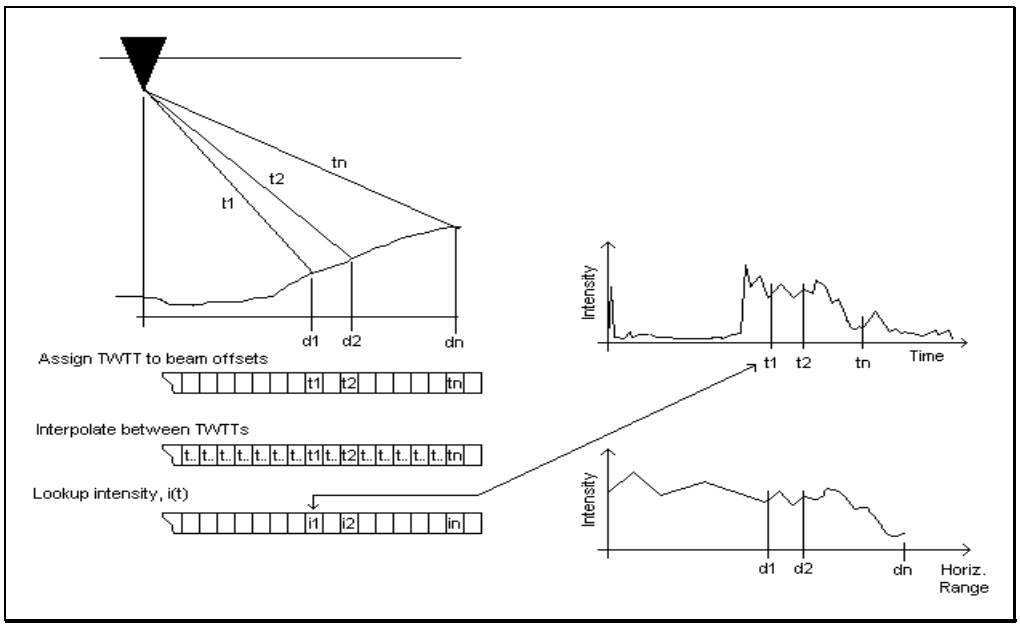

Figure 13. Slant-range to horizontal-range correction methodology. TWTTs are interpolated between known beam across-track offsets and are used to look-up intensities in the slant-range time series in order to populate the horizontal-range swath.

To view the results of the above operations, it is desirable to choose areas with significant topographic features to stress the limitations of the flat seafloor assumption and highlight the benefits of proper slant-range correction of backscatter data. A small example was chosen from the test dataset; along-track and across-track profiles of the area are shown in Figure 14. The area was chosen due to the presence of large outcrops of rock and presence of a sloped seafloor (refer to Figure 15).

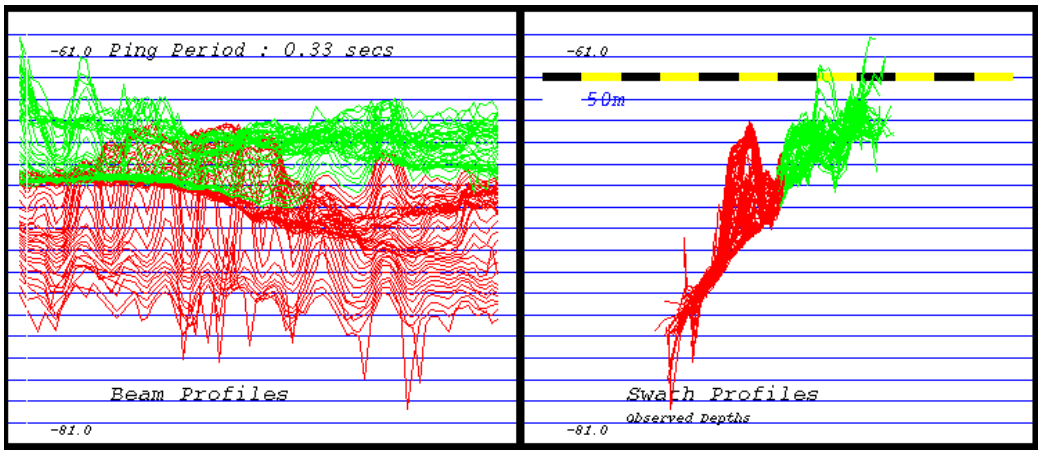

Figure 14. Along and across-track profiles of sample area. Water depths in this area range from approximately 65 to 75 metres with a typical swath width of 300 metres. All beams past 60° were filtered during the conversion process due to very poor quality soundings in the outer beams (following typical data cleaning procedures onboard the Rainier).

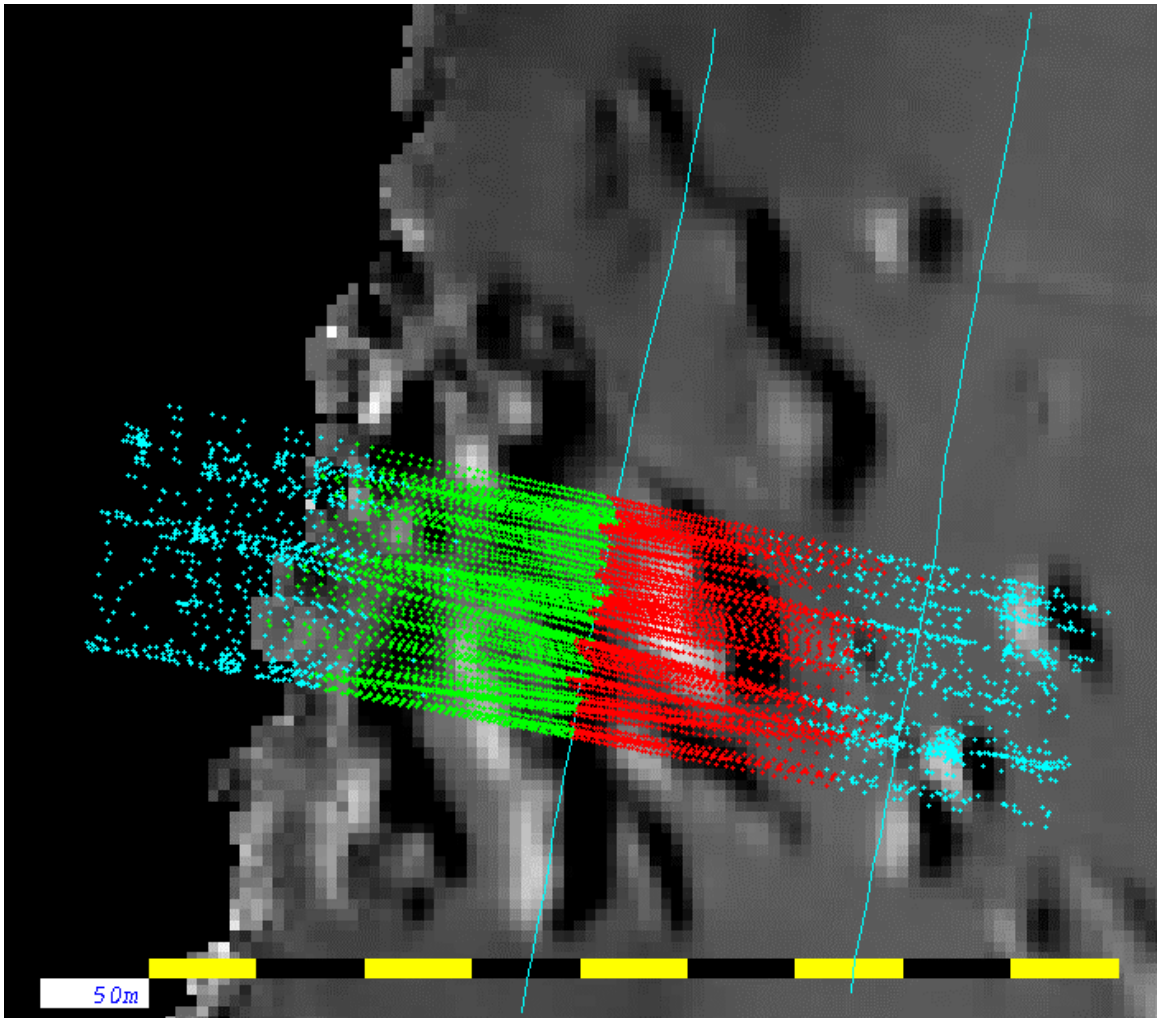

Figure 15. Sun-illuminated DTM of selected area (5 metre pixel resolution). North is oriented towards the top of the page. This subsection is from the southwestern portion of the study area (cf. Figure 12).

Images of the acoustic backscatter were prepared using both registration techniques and are shown in Figure 16. In this set of imagery, consecutive lines of data are simply stacked in time (time progressing down the page, port is to the right, starboard to the left) thus targets may suffer from along-track smearing and compression due to yaw of vessel. The effect is similar in both images, thus is negligible for the purposes of this illustration. Note that in the images created using the flat seafloor assumption that the data at nadir are noise due the nulls in the dedicated port and starboard receive beams at nadir. The software used to perform the flat seafloor correction ignored this fact and incorrectly stitched in low signal-to-noise data from outside the beam pattern. In the properly registered images, the nadir area is left empty, respecting the nadir insensitivity inboard of the edge of both the port and starboard sidescan beams (which roll with the vessel).

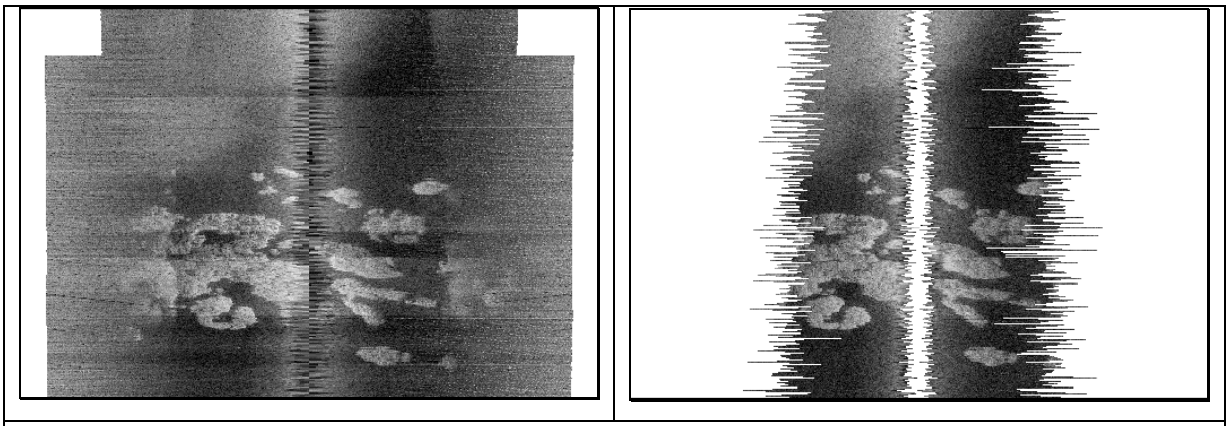

Figure 16. Flat seafloor assumption vs. slant-range correction with the bathymetric profile (on the left and right, respectively). Note that the trace data past the first multiple have been discarded in the image to the right while being preserved in the initial imagery prepared using a flat seafloor assumption.

To the naked eye, there is little difference in the pair of images in Figure 16; however, an increase in scale betrays the failings of the flat seafloor assumption by clearly demonstrating the compression of upslope targets to starboard (refer to Figure 17). In this example, a rock outcrop has been displaced laterally by approximately 3 metres.

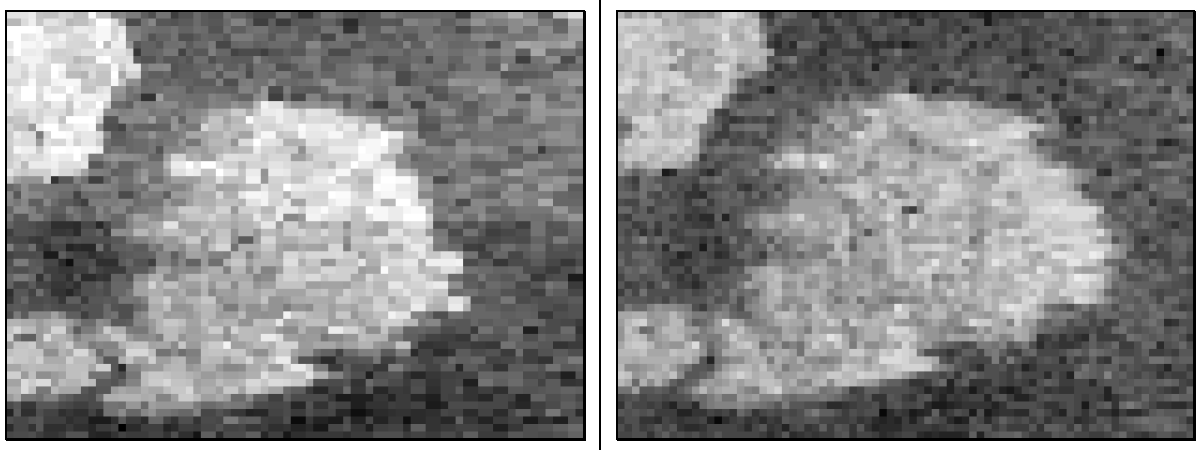

Figure 17. Target distortion and displacement due to flat seafloor assumption (flat seafloor assumption on the left, correct geo-registration on the right, nadir is towards right side of image). Note correction of power level artifact in right image. Vertical shift of target is due to mis-synchronization of bathymetry and sidescan packets (the flat seafloor algorithm registers all sidescan pings, whereas the second algorithm only registers those for which there is a corresponding bathymetry packet).

It is also possible to generate across-track intensity profiles using the beam-averaged data logged with the bathymetry data (one intensity per beam). The intensity associated with each receive beam is plotted using the beam's

across-track offset with the gaps in coverage between adjacent beams being filled by linear interpolation, effectively smearing the intensity values in the across-track direction. The same subset of data was chosen to illustrate the potential merits of using the beam-averaged intensities, as in Figure 18. There is no question that the trace data provide much better resolution (shown here at a 0.5 metre resolution), however, it is plausible that the beam-averaged intensities could potentially be used to fill in the gaps at nadir in the trace dataset (results from early attempts at this technique are shown later in this paper). At the very least, the generation of backscatter imagery from the beam-averaged intensities provides a check on the proper functioning of the slant-range correction algorithm as applied to the trace data.

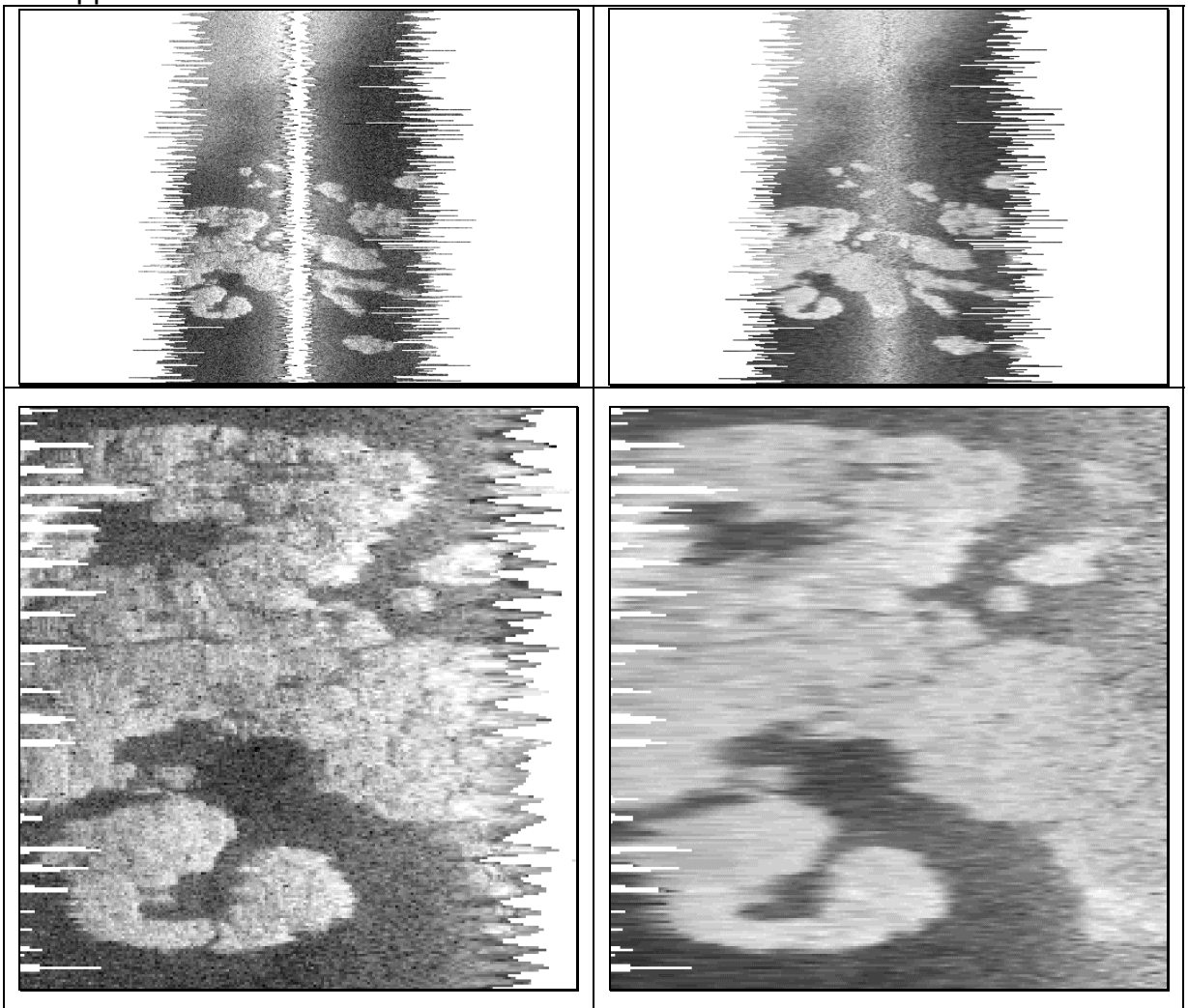

Figure 18. Comparison of trace backscatter to beam-averaged intensities (on the left and right, respectively). In the imagery produced from the beam-averaged data, object boundaries are smeared in the across-track direction. This results in an artificial enlargement of targets with object boundaries being extended by half the beam footprint in the worst-case scenario. This problem could potentially be overcome with an interpolation of higher-order between individual beam intensities.

Removal of Angular Response

A final radiometric reduction applied to the backscatter imagery is the removal of the along-track banding due to the angular response of the seafloor and the residual beam pattern of the sonar transducer. This is done by producing an average along-track angular response curve as a function of incidence angle. After computing the curve, the mean of the curve is calculated using the off-nadir responses and is then used to reduce the absolute angular response to relative corrections that must be applied as a function of incidence angle (e.g. suppress nadir by 3 dB as opposed to removing 60 dB, refer to Figure 19). The mean along-track response was computed for a survey line that passed over a relatively featureless portion of the seafloor in the area and is shown in Figure 19 for both the trace and beam-averaged data. Slant-range corrected imagery were produced both with and without removal of the angular response, as in Figure 20.

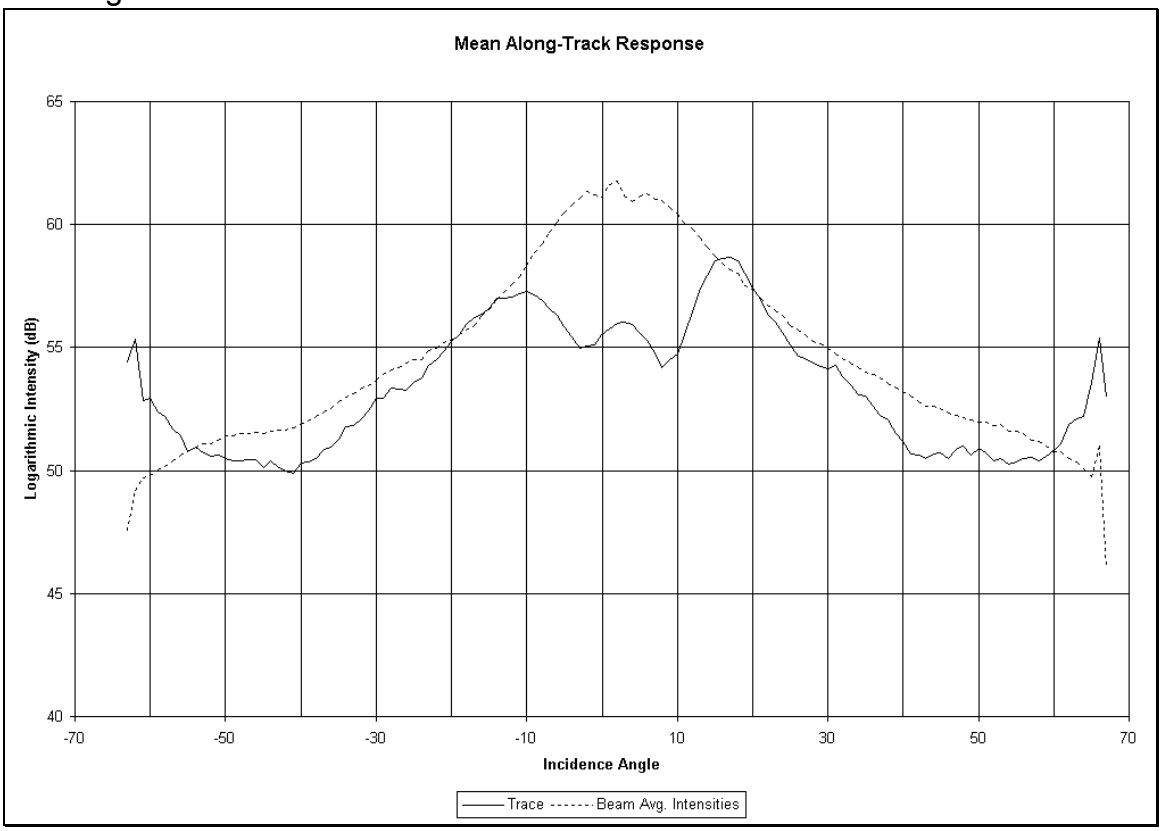

Figure 19. Mean along-track angular response curves of trace and beam-averaged intensities. Note that there should exist a null at nadir in the trace data curve, however, this is not seen in this plot due to the lack of roll stabilization and that the inboard edges of the port and starboard sidescan receive beams occasionally approach nadir.

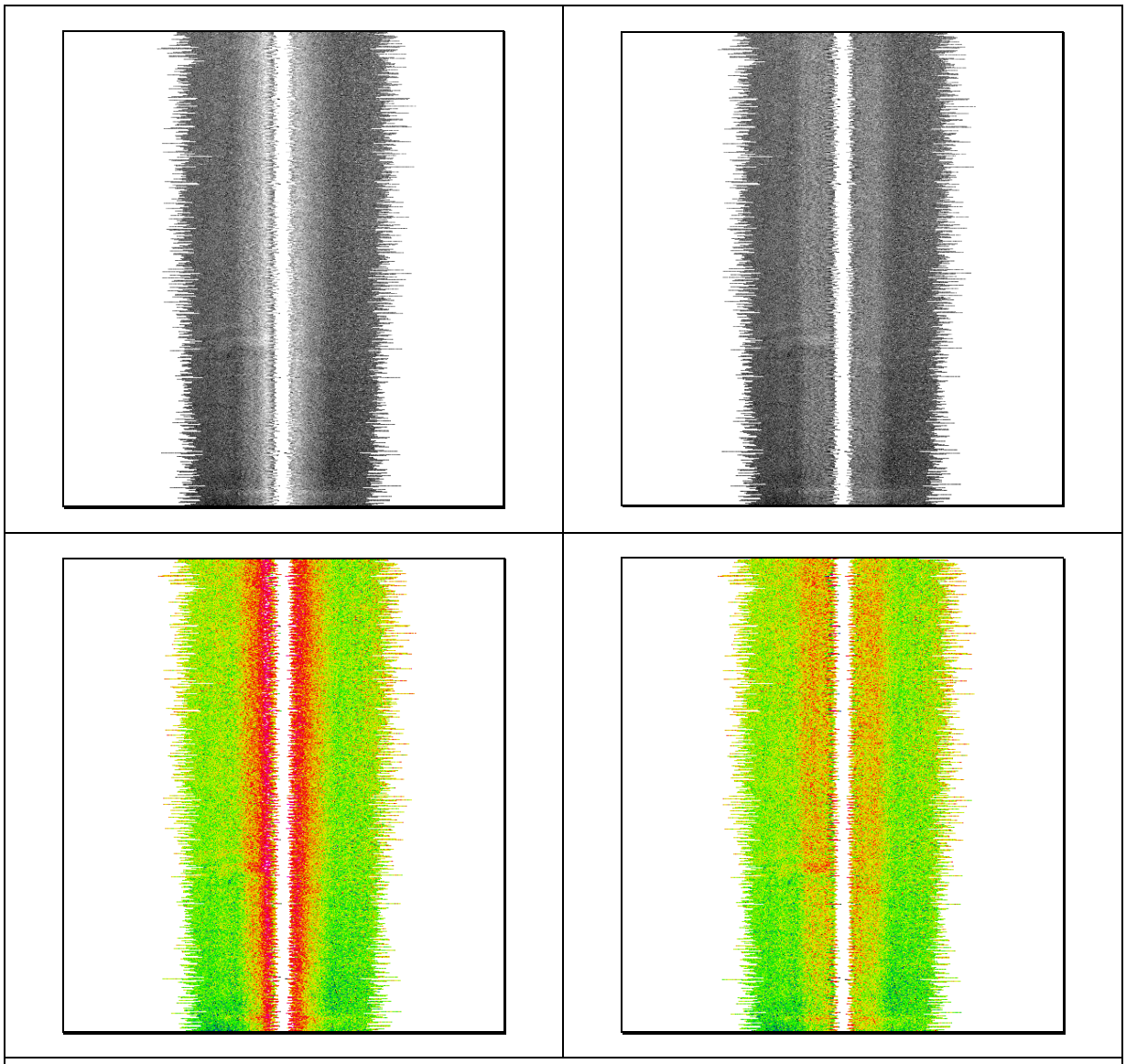

Figure 20. Beam pattern filtering of trace data (raw data on left, filtered on right). Raw images are shown in the left hand column, while filtered images are shown in the right; images are shown in greyscale and pseudo-colour to highlight the effect of the beam pattern removal.

Referring to Figure 20, it is evident that the majority of the angular response has been suppressed, however, a residual component remains in the inboard sections of the horizontal-range data. Complications are potentially due to the following conflicting facts:

1. The dominant component of the along-track response is the angular response curve of the seafloor, thus the along-track response should be computed relative to the seafloor normal, which varies with slope (for a given incident angle, what is the average response).
2. The residual beam pattern of the sonar transducer will roll with the system (since the system was not roll stabilized), thus the along-track response

should be computed relative to the sonar transducer (for a given beam, what is the average response).

3. The angular response shape changes with sediment type, so deviations from typical curves will remain in the data.

The angular response filtering improves the visual quality of the imagery to some extent though there remains further work to improve the performance of the filter. The same filtering can be done for the beam-averaged data with much better results, as shown in Figure 21.

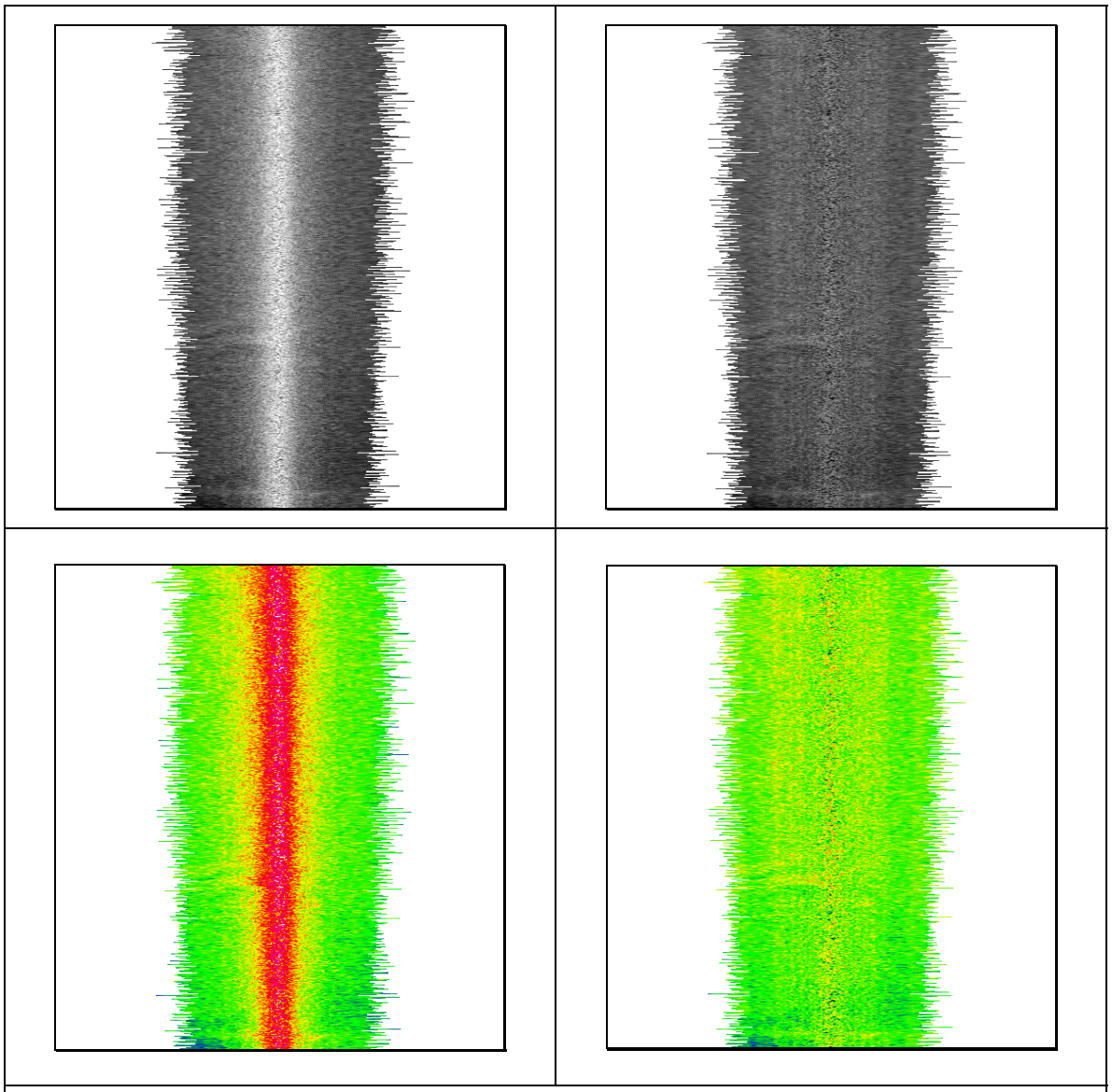

Figure 21. Beam pattern filtering of beam-averaged data (raw data on left, filtered on right). Again, pseudo-colour was used to highlight the suppression of the angular response.

Map Production

Mosaics of the slant-range corrected data were generated using existing OMG software. Initial results, with and without angular response corrections, are shown in the Figures 22 and 23.

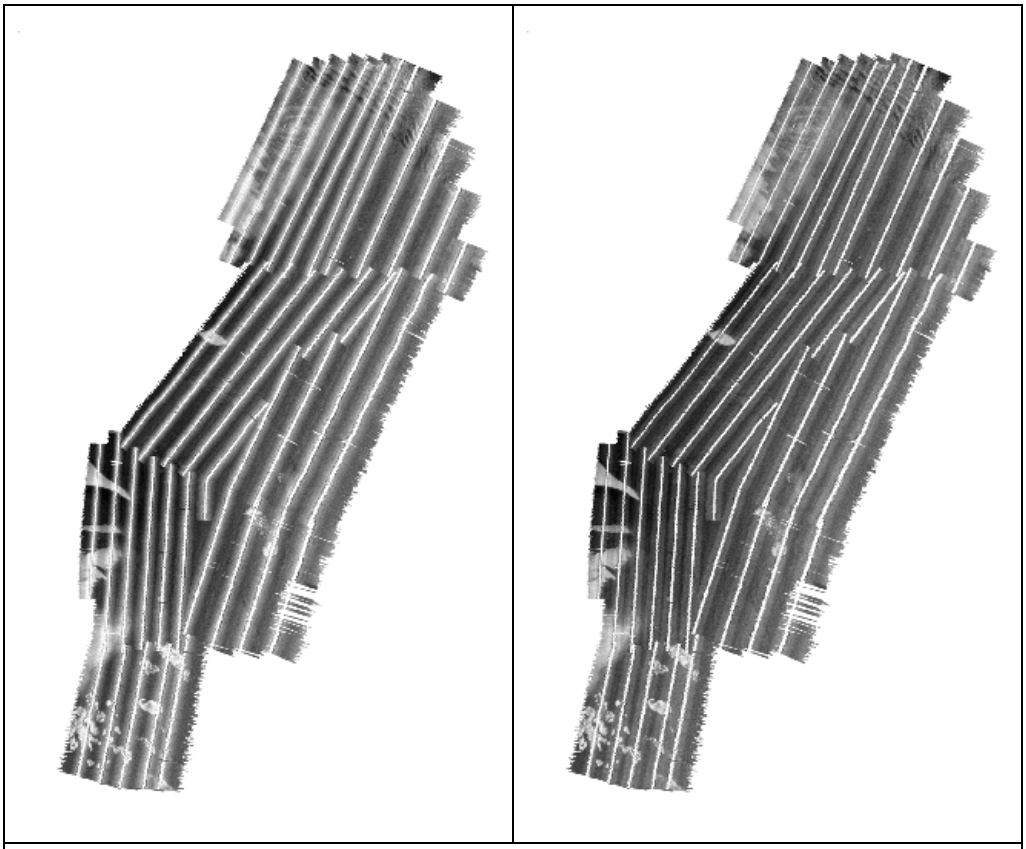

Figure 22. Mosaic of trace intensities (unfiltered image is on the left, angular response corrected image on the right). Pixel resolution is 2 metres.

As seen in Figure 22, all gain and power changes are corrected for, yielding a visually consistent image. The performance of the angular response filter is less effective than expected and further studies must be made into this (cf. section on Further Research). Again, there exists no data below the vessel track due to the nulls in the sidescan receiver beam patterns.

Map sheets were created for the beam-averaged data as well and are shown in Figure 23. In this case, the angular response curve performed as expected, removing most of the pattern except in cases of survey lines consisting mostly of featureless seafloor next to survey lines characterized by many topographic features. This is due to the dissimilarity of the angular response curves between the two lines since both lines are reduced to different mean levels. Thus the algorithm fails to bring the two datasets to a common level at the equidistant seam that joins the coverage of both lines. This could easily be

improved by shortening the length of the averaging window when computing the angular response curves and allowing a single line of data to have multiple angular response curves.

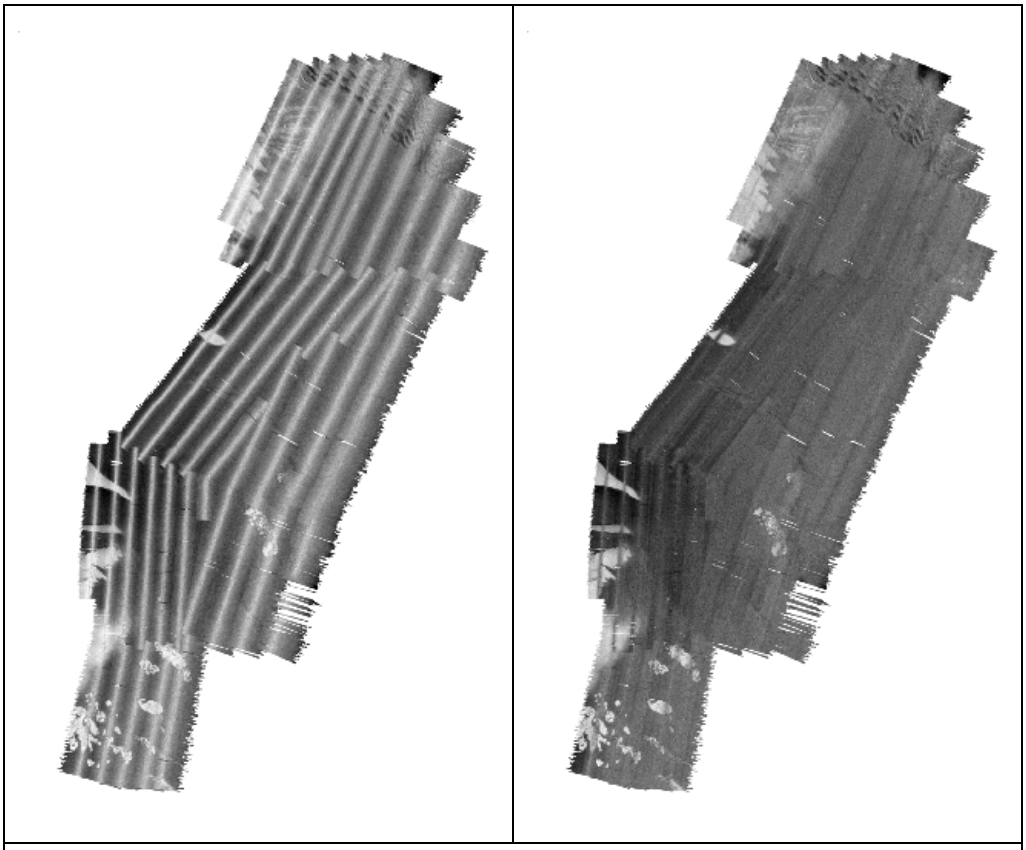

Figure 23. Mosaic of beam-averaged intensities (raw and beam pattern corrected). Pixel resolution is 2 metres.

Along with mosaics of trace and beam-averaged data, an attempt at combining the two datasets was made in which the nadir gap of the trace dataset was filled in with beam-averaged intensities. The different angular response curves for the trace data and beam-averaged intensities complicated the process of stitching the two data types together. This was overcome with slight modifications to the slant-range correction algorithm, allowing for the suppression (or boosting) of one signal to match the other by recalculating the mean of the angular response curve and determining the additive constant required to match the means (this constant being added to the corrective offsets applied as a function of incidence angle). Results of the blending of data types are shown in the Figure 24, along with the original dataset (flat seafloor assumption, no radiometric corrections applied for power, gain or angular response).

Figure 25 emphasizes the effectiveness of the radiometric and geometric corrections with two large-scale subsets from the maps of Figure 24. Even at this scale, the low resolution of the beam-averaged data is of little consequence and the beam-averaged data complements the trace intensities quite well. The

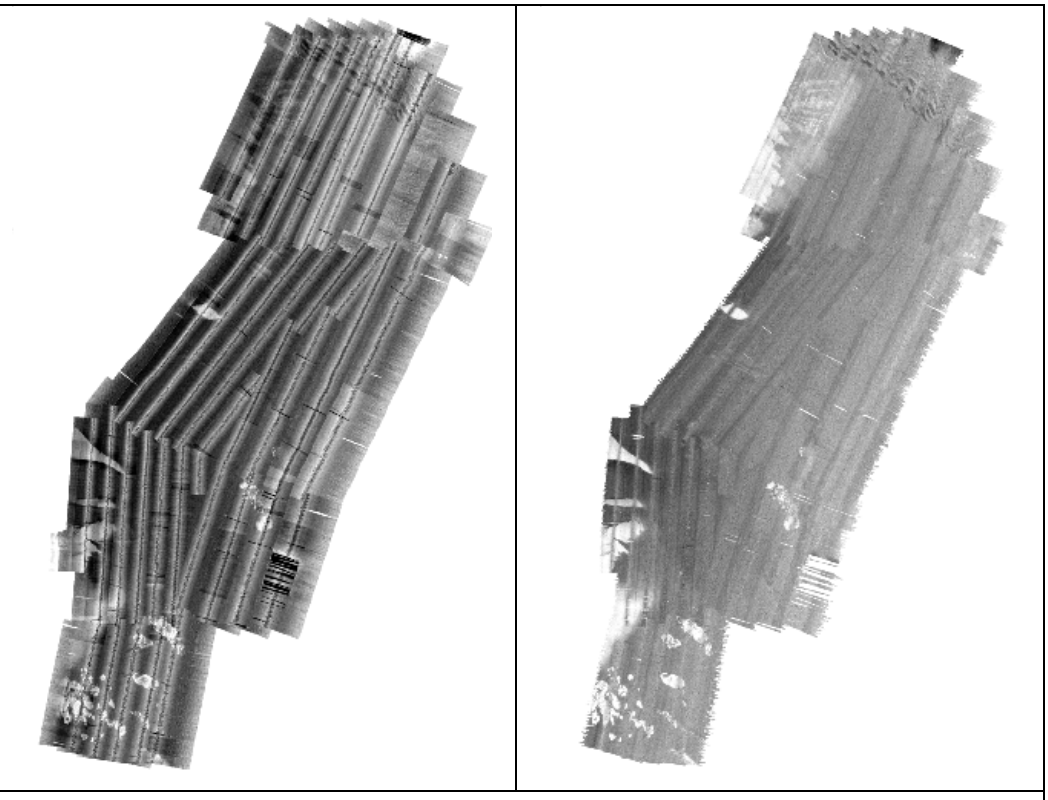

Figure 24. Initial map prepared using a flat seafloor assumption, and final map. The final map is a blend of trace intensities and beam-averaged intensities, and is fully corrected for power and gain settings as well as mean along-track angular response. Pixel resolution is 2 metres.

different resolution of both data types becomes an issue at larger scales, such as in Figure 18. As mentioned earlier, the removal of the angular response is sensitive to variations in topography and will perform poorly when neighbouring survey lines have vastly different angular response curves. This is particularly evident in the upper right image of Figure 25, where several survey lines join together at the top of the image. Again, this can be improved by shortening the time window over which the angular response curve is calculated.

FURTHER RESEARCH

Although resulting imagery is visually appealing, the maps cannot be analysed numerically given that the measured intensities have only partially been reduced to a measure of the true backscatter of the seafloor. Additional corrections remain:

1. The trace data must be normalized by pulse length to account for the ensonified area. This involves using the bathymetry to compute the varying grazing angles across-track.

2. The true source level must be determined and received intensities referenced to this value such that backscatter values can be used in an absolute manner.
3. The mean angular response curve of the trace data performs inadequately as a filter in the case of the trace data. An investigation must be made into the cause of the poor performance in hopes of developing a better method of removing the average along-track angular response.

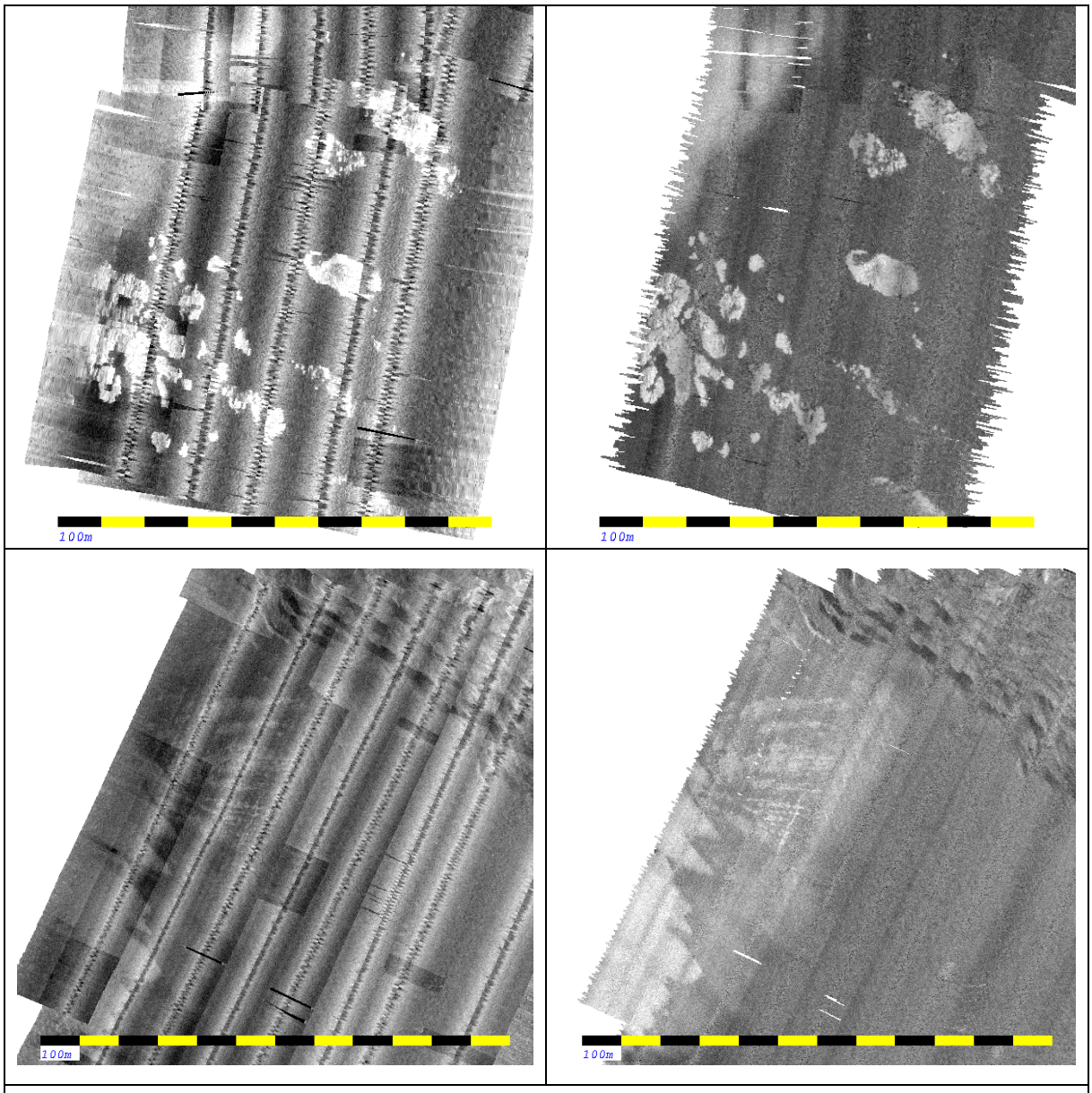

Figure 25. Large scale comparison of initial and final map products (left and right respectively). Radiometric artifacts due to power and gain have been completely compensated. The blended solution has the advantage of retaining the resolution of the trace data while incorporating the nadir backscatter from the beam-averaged intensities.

The value of registering trace data past the beam coverage should be examined, since the slant-range correction of the trace data currently ends at the multiple, i.e. 60 degrees off nadir. Although in this particular dataset the trace data past the multiple are by and large noise, it may prove useful to be able to register these data for applications when the sonar transducer is deployed on a tow body allowing for data collection with lower incidence angles. Although the bathymetry coverage would be limited to the swath width, it may be possible to geographically register the data using the bathymetry provided by neighbouring lines of data or an underlying DTM built from the bathymetry data. At the very least, the remainder of the signal can be slant-range corrected using a flat seafloor assumption past the edge of the useful bathymetry (or a simple slope model provided by the bathymetry). The errors introduced by the flat seafloor assumption lessen with distance, thus this last solution may prove reasonable in addition to being the simplest to implement.

While the focus of this work has been to extract useful backscatter data from SeaBat 8101 data with the single time-series trace data, it would be useful to expand all of the software developed up to this point to be able to handle the inclusion of snippet data (made possible by recent RESON firmware upgrades). A test data set collected with a SeaBat 8111 has been provided by D. Lockhart of Thales GeoSolutions and will be used in future research.

SUMMARY

The RESON SeaBat 8101, as installed on the launches of the NOAA ship Rainier, can log acoustic backscatter in two formats: a time-series of intensities (provided by the sidescan option), and beam-averaged intensities (associated with each bathymetric receive beam). Unfortunately, existing software tools only perform a flat seafloor assumption on the data provided via the sidescan option. Further to this, the raw backscatter data is uncorrected for variations in transmit power and receiver gain.

Software tools have been developed to convert the Rainier SeaBat data (logged in XTF) into the OMG format. Once in the OMG format, it is possible to perform a proper slant-range correction by registering portions of the intensity time-series using the bathymetric profile. Algorithms were developed to correct the intensities for power and gain settings (as logged by the sonar). In addition, existing software in the OMG was updated to compute the average along-track angular response of the trace and beam-averaged data. These radiometric corrections can be applied during the slant-range correction process, resulting in horizontal-range backscatter that is geometrically correct and radiometrically consistent across the dataset.

The software developed at this point is capable of producing mosaics of acoustic backscatter both from the trace and beam-averaged data. A third option was investigated that allow for the blending of the two sources of data within a single survey line. This was done to overcome the lack of data at nadir in the

trace dataset (due to a null at nadir in the sidescan receive beams, resulting in a gap in any backscatter data directly below the vessel track). The blended product preserves the high-resolution backscatter provided by the trace data away from nadir and fills in the gap at nadir with the beam-averaged data.

Further work will involve further reducing the backscatter data for pulse width and grazing angle, in addition to refining the removal of the angular response curve as it performs poorly for the trace data at this point. Finally, the last radiometric correction is to reference all intensity values to a currently unknown source level such that they can be used in an absolute manner. Other future research will focus on geo-registering the trace data past the end of the bathymetric coverage, in addition to adaptation of software to the inclusion of snippet data, as provided by recent firmware upgrades by RESON.

ACKNOWLEDGEMENTS

This research has been made possible through the funding of the U.S. Geological Survey. Thanks to Captain James Gardner (NOAA) for accommodations onboard the Rainier during field trials and collection of the test data set. Finally, special thanks to Burr Bridge (RESON, USA) and Jack Riley (NOAA) who both provided insight into the finer points of the RESON and XTF data formats.

REFERENCES

Hughes Clarke, J.E., L.A. Mayer, and D.E. Wells (1996). "Shallow-Water Imaging Multibeam Sonars: A New Tool for Investigating Seafloor Processes in the Coastal Zone and on the Continental Shelf." Accepted for publication 7 March 1996 in *Marine Geophysical Researches.*

Hughes Clarke, J.E. (1997). Field Laboratory using RESON SeaBat 9001 and Seatex MRU-6. http://www.omg.unb.ca/~jhc/HYDRO_I_97/, February 2002.

Hughes Clarke, J.E. (1998). Multibeam Sonar Imaging. Lecture 10, 1998 Coastal Multibeam Sonar Training Course. Dartmouth, Nova Scotia, 20-24 April, 1998.

Lockhart, D., R. Pawlowski and E. Saade (2001). Multibeam Based Mapping of Fisheries Habitats in Alaska: Innovations in Imagery Products. http://www.ccom-jhc.unh.edu/shallow/abstracts/multibeam_fisheries.htm, Feb 2002.

RESON (2000). *SeaBat 8101 Multibeam Echosounder System*. Operator's Manual, v. 2.20, Goleta, California.